frontiers in Earth Science

TYPE Original Research
PUBLISHED 24 July 2026
DOI 10.3389/feart.2026.1839921

OPEN ACCESS

EDITED BY
Min Luo,
Fuzhou University, China

REVIEWED BY
George E. Kapellos,
Massachusetts Institute of Technology, United States
Kaltham Ismail,
University of Khorfakkan, United Arab Emirates
Kiefer Forsch,
University of Southern California, United States

*CORRESPONDENCE
Margaret Bernish,
mbernish@gmail.com
Jongsun Kim,
jongsun.kim@utrgv.edu

RECEIVED 26 March 2026
REVISED 20 May 2026
ACCEPTED 30 May 2026
PUBLISHED 24 July 2026

CITATION
Bernish M, Gao M, Kim J, Pasquier B and Inomura K (2026) Using a cell flux model to investigate phytoplankton growth and macromolecular allocation under iron limitation.
Front. Earth Sci. 14:1839921.
doi: 10.3389/feart.2026.1839921

Using a cell flux model to investigate phytoplankton growth and macromolecular allocation under iron limitation

Margaret Bernish[1]*, Meng Gao[1], Jongsun Kim[2]*, Benoit Pasquier[3] and Keisuke Inomura[1]

[1]Graduate School of Oceanography, University of Rhode Island, Narragansett, RI, United States, [2]School of Earth, Environmental, and Marine Sciences, University of Texas Rio Grande Valley, Brownsville, TX, United States, [3]School of Mathematics and Statistics, University of South New Wales, Sydney, NSW, Australia

Global biogeochemical models are powerful tools used to interpret observations and empirical data, create hypotheses, and make predictions. Many of these models, however, represent marine microbes as static stoichiometric reactions that convert nutrients into biomass. To better constrain the biological processes that control nutrient cycling in the global ocean, we extend the Cell Flux Model of Phytoplankton to explore the impact of dissolved iron concentration on the allocation of macromolecules and elemental ratios within phytoplankton cells. This model is supported by data obtained from a range of incubation experiments conducted with phytoplankton of varying species and size categories. Model output is applied globally to highlights the effects of iron and light availability and physiological adaptation on the distribution of open ocean and neritic phytoplankton taxa. This research aims to elucidate the role of phytoplankton physiology within biogeochemical cycles, allowing for better characterization of marine microbial distribution and elemental makeup for interpretive and predictive models.

KEYWORDS
biogeochemical, iron limitation, marine ecology, microbial ecoclogy, phytoplankton

Highlights

- A mechanistic model of phytoplankton is used to investigate the effect of iron limitation on cellular macromolecular allocation.
- The interacting effects of temperature and light on iron-limited phytoplankton physiology are incorporated into the model using existing formulations.
- Growth and allocation patterns of an oceanic phytoplankton taxon are evaluated on a global scale using modeling output and satellite data.

1 Introduction

Phytoplankton play important parts in the biogeochemical cycling of carbon and other nutrients, contributing to almost 50% of the global net primary production

despite contributing to only 1% of the total photosynthetic biomass (Field et al., 1998). Variations in elemental proportions within phytoplankton are known to drive large-scale patterns of the stoichiometric makeup of organic matter (Finkel et al., 2016; Liefer et al., 2019). Shifts in nutrient input fluxes, surface ocean chemistry, and ocean circulation as a result of anthropogenic climate change will influence the availability of macro- and micro-nutrients in the future, driving changes in global marine microbial ecology and the export of organic matter (Eppley and Peterson, 1979; Steinacher et al., 2010).

Due to its flexible redox chemistry, iron is used within electron transfer reactions in both photosystems (Schoffman et al., 2016). In the ocean, dissolved iron sticks to sinking particles and is rapidly scavenged from the water column, rendering upwelled waters relatively low in iron compared to macronutrients (Tagliabue et al., 2014). Thus, despite only being required in trace amounts, iron limits primary production in approximately a third of the global surface ocean (Boyd et al., 2007; Breitbarth et al., 2010). In addition, other environmental factors, namely, light and temperature, have been demonstrated to influence the physiological responses of phytoplankton to iron limitation (Jabre and Bertrand, 2020; Sunda and Huntsman, 2011). For example, decreased light levels and photoperiods drive an increased cellular demand for iron, a result of the cell up-regulating the capacity of its photosynthetic machinery (Sunda and Huntsman, 1997; Feng et al., 2010). However, current earth system models do not explicitly represent the interacting effects of light, temperature, and iron concentration on cell physiology.

In this study, we extend a coarse-grained cellular physiology model to resolve the relationship between dissolved iron concentrations and macromolecular allocation. This model accounts for important physiological responses to different growth conditions, using two parameters optimized for various phytoplankton taxa. We implement the model on a global scale using gridded dissolved iron concentrations and observe how environmental factors (e.g., light intensity and temperature) affect the macromolecular allocation and elemental composition of neritic and oceanic phytoplankton taxa. Through focusing on the physiological context provided by model output, we interpret the relationship between micronutrient concentration and phytoplankton growth; namely, how macromolecular allocation is affected by external iron concentrations in conjunction with other environmental factors.

There has been a considerable effort by researchers to extend the breadth of ecological and biogeochemical models in order to describe how ocean systems have and will continue to change under various climate scenarios. However, linking limited incubation experiments to larger-scale models and understanding the effects of multiple stressors on phytoplankton physiology is a major challenge (Follows et al., 2007). This research will advance the predictive power of earth system models through providing a mechanistic understanding of the microbial processes that underlie the biological cycling of iron and other nutrients.

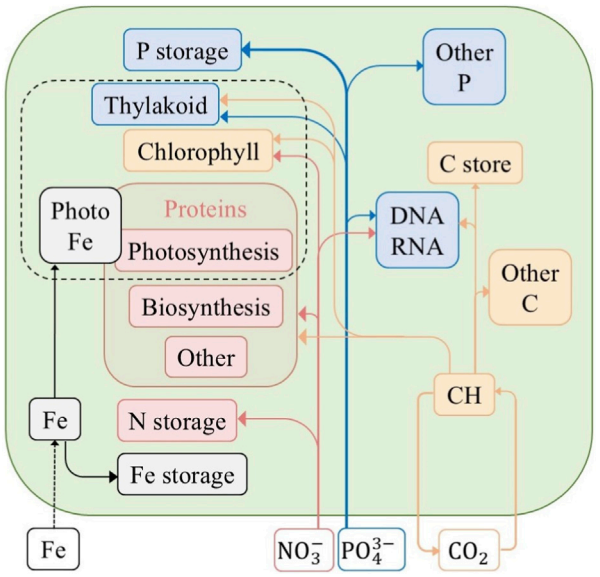

FIGURE 1
Schematic representation of the Cell Flux Model of Phytoplankton, depicting allocation of C, N, P, and Fe to key macromolecular pools. Arrows represent elemental fluxes (yellow, C; red, N; blue, P; black, Fe). Yellow, red, blue, and black boxes represent molecules that mainly influence C, N, P, and Fe budgets, respectively. Dashed box represents photosynthetic molecules. CH (carbohydrates) and P thyla represent the precursor molecules in thylakoid membranes. Schematic is derived from Armin and Inomura, 2021.

2 Materials and methods

2.1 The Cell Flux Model of Phytoplankton

The Cell Flux Model of Phytoplankton (hereby referred to as CFM-Phyto; Figure 1) is a mechanistic model used to estimate and quantify the growth rate, stoichiometry, and macromolecular allocation of phytoplankton under different environmental conditions (Inomura et al., 2020). Essential elements, such as carbon, nitrogen, and phosphorus, are assigned to major macromolecular groups, including proteins, RNA, DNA, and photosynthetic machinery, each with their own distinct stoichiometric ratios. CFM-Phyto has been demonstrated to reflect the observed growth rates and elemental stoichiometry of various species of phytoplankton (Inomura et al., 2020). It has also been used to estimate the temperature and light dependencies of stoichiometric ratios, as well as to predict the stoichiometric ratios of phytoplankton based on remote sensing data (Armin and Inomura, 2021; Kim et al., 2022; Tanioka and Matsumoto, 2020).

2.2 Calculation of μ

Before determining the cell's resource allocation and elemental makeup, the specific growth rate must be calculated. We first assume a steady state condition in which the change of cellular iron

concentration over time is equal to 0. As a result, the rate of iron uptake (V_{Fe}, in mol Fe (mol C d)$^{-1}$) is balanced by the growth rate (μ, in d^{-1}) multiplied by the cellular iron Q_{Fe}, in mol Fe (mol C)$^{-1}$.

$$\frac{dQ_{Fe}}{dt} = V_{Fe} - \mu Q_{Fe} = 0 \quad (1)$$

Cellular iron uptake is linearly proportional to the extracellular iron concentration with an affinity parameter a_{Fe} (in $\frac{mol\,Fe}{\mu M\,Fe\,mol\,C\,d}$):

$$V_{Fe} = a_{Fe}[Fe] \quad (2)$$

Major iron allocations are to photosystems, enzymes involved in nitrogen fixation (nitrogenase), and other pools, including storage (Saito et al., 2011). As this version of CFM-Phyto focuses on non-N_2 fixing phytoplankton, we assume that the allocation to nitrogen fixation enzymes is negligible. We also assume that iron storage is small. These assumptions lead to a further assumption that the cellular iron is approximate to the iron allocated to photosystems, described by Equation 3:

$$Q_{Fe} \sim Q_{Fe}^{Pho} \quad (3)$$

Relating the allocation of iron to photosystems to the investment in chlorophyll yields the following equation (Inomura et al., 2022):

$$Q_{Fe}^{Pho} = A_{Pho}^{Fe} Q_C^{Chl} \quad (4)$$

where A_{Pho}^{Fe} is a factor that represents the moles of iron required for each mole of chlorophyll (in units mol Fe (mol C in chlorophyll)$^{-1}$).

While the pigment to photosystem ratio has been observed to vary, this simplification allows for an explicit, mechanistically motivated representation of iron limitation (Strzepek et al., 2019). Q_C^{Chl} represents the empirically-observed linear relationship between cellular chlorophyll to carbon ratio and growth rate under a given light intensity:

$$Q_C^{Chl} = \frac{1+E}{v_I}\mu + \frac{m}{v_I} \quad (5)$$

where E (dimensionless) represents growth-rate-dependent respiration, m (in d^{-1}) represents maintenance respiration (Inomura et al., 2020), and v_I represents the rate of carbon fixation in mol C (mol C in chlorophyll)$^{-1}$ d^{-1} at light intensity I:

$$v_I = v_I^{max}\left(1 - e^{A_I I}\right) \quad (6)$$

where v_I^{max} represents the maximum carbon fixation rate per chlorophyll in mol C (mol C in chlorophyll)$^{-1}$ d^{-1} and A_I represents a coefficient characterizing the turnover time of the photosynthetic unit (Cullen, 1990). Inserting Equations 2, 4 and 5 into Equation 1 yields the following quadratic relationship between Q_{Fe} and μ:

$$-\frac{A_{Pho}^{Fe}(1+E)\mu^2}{v_I} - \frac{A_{Pho}^{Fe} m\mu}{v_I} + a_{Fe}[Fe] = 0 \quad (7)$$

The solution for μ is obtained by solving the standard quadratic equation,

$$\mu = \frac{-b + \sqrt{b^2 - 4ac}}{2a} \quad (8)$$

where $a = -\frac{A_{Pho}^{Fe}(1+E)}{v_I}$, $b = -\frac{A_{Pho}^{Fe} m}{v_I}$, and $c = a_{Fe}[Fe]$.

2.3 Data and parameter optimization

We compiled data from 9 published papers on phytoplankton growth under iron-limited conditions (Table 1). For each of these datasets, two parameters used in the calculation of cell growth under iron limitation, a_{Fe} and A_{Pho}^{Fe} (Equation 7), were optimized using the Metropolis-Hastings algorithm, a Markov Chain Monte Carlo (MCMC) method that introduces perturbations to initial estimates and converges to values that best fit the data (Metropolis et al., 1953; Hastings, 1970). The method consists of two parts: generation of parameters and testing. In the testing part, we compute the likelihood ratio based on the model data fit and generate a random value between 0 and 1. If the updated likelihood ratio is greater than the previous likelihood ratio, we will replace the parameter set with the newly generated ones, and we repeat the procedure (more detailed description of the overall process is in Inomura et al., 2020). In our parameterization, the number of iterations was 10,000, which was sufficient in getting a visually decent model-data fit (Figure 2). Optimized values for a_{Fe} and A_{Pho}^{Fe} can be found in the Supplementary Information (Supplementary Table S1).

After finding parameter values that yield the closest fit to the observed data, we ran simulations under increasing iron concentrations (ranging from 0 to 8 nM, with increments of 1e-3 nM), in order to observe the effect of iron concentration on the cellular carbon allocation to four categories of macromolecular pools: molecules involved in biosynthesis, photosynthesis, essential cellular structure, and storage. For each species, the model was run using optimized parameters, as well as constant irradiance and temperature values reflective of those used in each culture study (Table 1).

2.4 Functional macromolecular allocation

After calculating the growth rate (Section 2.2), CFM-Phyto was extended to resolve the interacting effects of iron limitation, temperature, and light intensity on functional carbon-based allocation (Inomura et al., 2020). This iteration of the model takes in the growth rate (Equation 8), light intensity (Equation 6), and temperature (Equation 9), using these factors to predict functional macromolecular allocation. Key assumptions include: (1) A saturating relationship between light intensity and C fixation rate (Equation 6), (2) Fixed composition of photosystems, (3) Linear relationship between the growth rate and biosynthetic proteins, and (4) Linear relationship between RNA, growth rate, and the quantity of proteins (Inomura et al., 2020).

Assumption (1) follows a commonly used formula based on target theory (Geider et al., 1998; Cullen, 1990). Assumption (2) indicates that the composition of chloroplasts is constant due to a lack of data needed to constrain their molecular variation. Whereas this assumption may not strictly reflect reality, it simplifies the model while providing a close fit for the overall elemental stoichiometry of the cell (Inomura et al., 2020). Assumption (3) follows a simple idea: biosynthetic protein is required to create biomass for new cells. Thus, to grow faster, the cells need more biosynthetic protein. This assumption is based on the observed relationship in heterotrophic bacteria (Scott et al., 2010; Bremer and Dennis, 1996). This relationship can also be inferred from the generally observed pattern of phytoplankton growth: increasing

TABLE 1 List of phytoplankton taxa used in this study.

Author(s)	Year	Species used	Light (μmol $m^{-2}s^{-1}$)	Temperature (°C)	Isolate
Sunda and Huntsman, 1995	1995	*E. huxleyi*	500	20	Oceanic
Sunda and Huntsman, 1995	1995	*P. calceolata*	500	20	Oceanic
Sunda and Huntsman, 1995	1995	*T. oceanica*	500	20	Oceanic
Sunda and Huntsman, 1997	1997	*T. weissflogii*	500	20	Neritic
Sunda and Huntsman, 1997	1997	*T. pseudonana*	500	20	Neritic
Sunda and Huntsman, 1997	1997	*P. minimum*	50	20	Neritic
Sunda and Huntsman, 1997	1997	*P. micans*	50	20	Neritic
Jabre and Bertrand (2020)	2020	*F. cylindrus*	50	6	Neritic
Jabre and Bertrand (2020)	2020	*F. cylindrus*	50	3	Neritic
Jabre and Bertrand (2020)	2020	*F. cylindrus*	50	1	Neritic

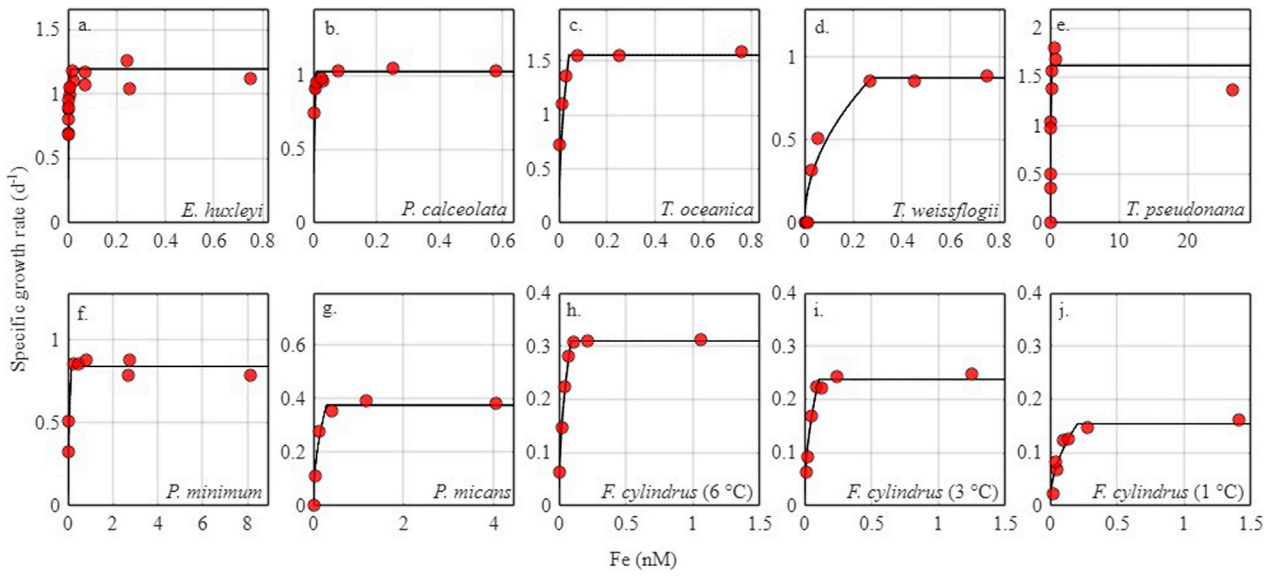

FIGURE 2
Observed (red circles) and predicted specific growth rates versus increasing dissolved iron concentrations using CFM-Phyto (black solid line) for **(a)** *Emiliania huxleyi* (Sunda and Huntsman, 1995), **(b)** *Pelagomonas calceolata* (Sunda and Huntsman, 1995), **(c)** *Thalassiosira oceanica* (Sunda and Huntsman, 1995), **(d)** *Thalassiosira weissflogii* (Sunda and Huntsman, 1997), **(e)** *Thalassiosira pseudonana* (Sunda and Huntsman, 1997), **(f)** *Prorocentrum minimum* (Sunda and Huntsman, 1997) **(g)** *Prorocentrum micans* (Sunda and Huntsman, 1997), **(h)** *Fragilariopsis cylindrus* grown at 6 °C (Jabre and Bertrand, 2020), **(i)** *Fragilariopsis cylindrus* grown at 3 °C (JJabre and Bertrand, 2020), **(j)** *Fragilariopsis cylindrus* grown at 1 °C (Jabre and Bertrand, 2020).

growth rates require increased protein content and, as a result, an increase in the cell's overall N:C ratio (Rhee, 1978; Chalup and Laws, 1990). This assumption is also supported by a recent proteomics study that shows linearly increasing levels of proteins related to biomass synthesis (Jahn et al., 2018). Assumption (4) is based on the observed linear relationship between the ratio of RNA to protein with the growth rate in heterotrophic bacteria and in phytoplankton (Scott et al., 2010; Nicklisch and Steinberg, 2009). We used previously defined parameters based on the culture of *Synechococcus linearis*, which were previously represented in regional and global patterns of observed elemental stoichiometry (Healey, 1985; Inomura et al., 2022; Liefer et al., 2024).

We also incorporate the effects of temperature on cellular functional allocation. The Arrhenius rate constant is used to relate the ambient temperature on the rate of biosynthesis associated with cellular respiration and growth (Armin and Inomura, 2021):

$$Arr = e^{\frac{E_a}{R}\left(\frac{1}{T}-\frac{1}{T_{ref}}\right)} \quad (9)$$

where the activation energy (E_a) is equal to 70,000 J $(mol)^{-1}$, the universal gas constant R is set to 8.3 J mol^{-1} K^{-1}, and the reference temperature (T_{ref}) is set to 293 K (Taylor et al., 1997; Armin and Inomura, 2021). This rate constant is applied to the allocation of carbon to biosynthetic proteins through the

following equation (Armin and Inomura, 2021):

$$Q_C^{Pro-Bio} = \frac{A_{Bio}}{Arr} \times \mu \quad (10)$$

The rate constant is also applied to the allocation of phosphorus to RNA through the following equation:

$$Q_P^{RNA} = \frac{A_P^{RNA}}{Arr} \times \mu \times Q_C^{Pro} + Q_{P,min}^{RNA} \quad (11)$$

2.5 Global gridded light, temperature, and dissolved iron data

To implement CFM-Phyto on a global scale, we obtain global gridded satellite output of surface PAR and k_{dPAR} (obtained from the Suomi National Polar-orbiting Partnership's Visible Infrared Imaging Radiometer Suite) in order to calculate the 3D climatological average of light intensity in the upper ~100 m of the ocean (Son and Wang, 2015). To calculate the light intensity at depth z (I_Z, in μmol $m^{-2}s^{-1}$) given surface PAR (I_0), we use the following formulation Equation 10 (Morel, 1988):

$$I_z = I_0 e^{-k_{dPAR}z} \quad (12)$$

where k_{dPAR} represents the diffuse attenuation coefficient of PAR (in m^{-1}).

The upper ~100 m grid boxes of ocean temperature were obtained from the Reagan et al., 2024 product and averaged over depth (Reagan et al., 2024). The climatological values of temperature and light used as input for CFM-Phyto are located in the Supplementary Information (Supplementary Figure S4). Global gridded dissolved iron concentrations were obtained from a data-driven dissolved iron climatology and averaged over the upper 100 m (Huang et al., 2022) (Supplementary Figure S3).

3 Results and discussion

3.1 Model validation

Two major growth phases are inferred from the model output: a rapidly increasing growth rate, where growth is limited by iron availability, and a carbon-limited growth phase, where additional iron input does not stimulate growth. Under low iron concentrations, the increase in cellular demand for iron is attributed to an increase in iron uptake, driving an inferred nonlinear relationship between μ and iron as seen in the iron-limited phase of growth (Figure 3C).

Under severe iron limitation, cells allocate a large fraction of carbon to storage molecules (Supplementary Figure S1). As iron availability increases, storage carbon declines while photosynthetic and biosynthetic allocation increases to support faster growth. Once cells enter the carbon-limited phase, storage is depleted and carbon is primarily directed toward growth-supporting machinery. This pattern is consistent with proteomic evidence (Jahn et al., 2018; Zavřel et al., 2019; Faizi et al., 2018).

CFM-Phyto appears to reproduce the observed growth rates in phytoplankton across different Fe concentrations (Figure 3). Maximum specific growth rates, as well as the concentration of Fe required to reach them, vary among species and size classes, reflecting the physiological diversity between phytoplankton taxa. The open ocean isolates *Emiliania huxleyi*, *P. calceolata,* and *Thalassiosira oceanica* saturate at the lowest iron concentrations, reflecting their adaptation to iron-limiting conditions (Sunda and Huntsman, 1995).

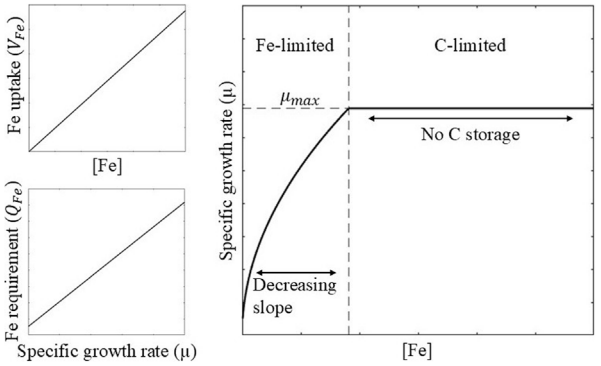

FIGURE 3
Schematic showing two major growth phases of phytoplankton under increasing iron concentration: iron-limited growth, where the slope of growth rate versus iron decreases until it reaches a maximum growth rate (μ_{max}), and carbon-limited growth, where all of the cellular carbon is allocated to biosynthetic and photosynthetic molecules in order to support the maximum growth rate.

3.2 Macromolecular allocation and elemental stoichiometry

Carbon-based macromolecular allocation provides a physiological explanation for the changes in elemental stoichiometry. The overall elemental stoichiometry of the cell is dependent upon the relative abundance of each macromolecular pool and its respective stoichiometric makeup. Under iron limitation, the cell allocates a significant portion of its cellular carbon to storage, lowering its total N:C ratio (Figure 4a–4c). In contrast, the cell allocates more carbon to biosynthesis when iron is replete, increasing its total protein content and, as a result, its overall N:C ratio (Figure 4b–4d).

In CFM, cellular nitrogen is allocated to essential molecules, which represent a constant pool of non-photosynthetic phospholipids, DNA, ATP, and ADP (molecules essential for maintenance and growth), photosynthesis, and biosynthesis (Inomura et al., 2020). The photosynthetic apparatus, which consists of proteins, chlorophyll, and lipid-rich thylakoid membranes, has a relatively high N:C ratio (Geider and La Roche, 2002). Increasing growth rates are accompanied by higher fixed C requirements, leading to increased photosynthetic molecules and higher overall N:C ratios within the cell (Inomura et al., 2020). Under iron limitation, CFM output suggests that oceanic species (e.g., *Emiliania huxleyi, P. calceolata*, and *Thalassiosira oceanica*) have higher N:C ratios than their neritic counterparts (Figure 4c). This physiological difference, as suggested by CFM and supported by culture studies, is the result of their relatively low iron requirements, which allow

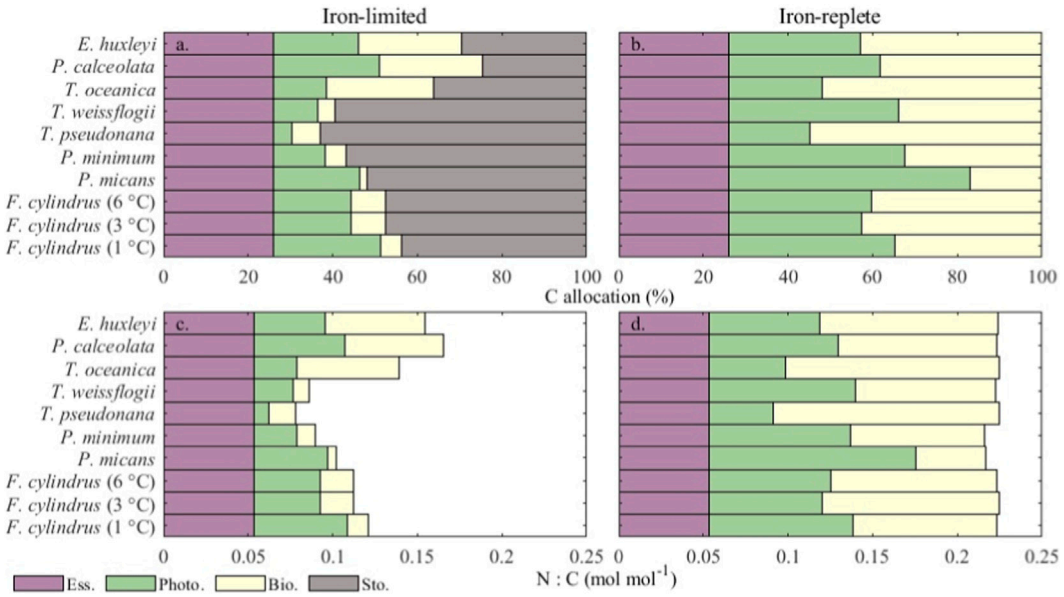

FIGURE 4
Carbon-based **(a,b)** and nitrogen-based (per cellular C; **(c,d)** functional allocation under iron-limited (left [dFe] = 0.001 nM) and iron-replete (right; [dFe] = 1 nM) conditions.

them to survive in the iron-depleted open ocean (Sunda and Huntsman, 1995).

3.3 Interactions between iron concentration, light, and temperature

Light and temperature impose constraints on phytoplankton growth and physiology: the former through limiting photosynthetic activity, and the latter through limiting biosynthetic processes (Schoffman et al., 2016; Armin and Inomura, 2021). Increasing temperatures have been demonstrated to increase the metabolic efficiency of biosynthetic processes within phytoplankton (Regaudie-de-Gioux & Duarte, 2012). In a previous iteration of CFM-Phyto that incorporates temperature into calculations of carbon-based allocation, it was found that the number of biosynthetic molecules needed to maintain a specific, constant growth rate is inversely related to temperature (Armin and Inomura, 2021). Here, we examine the response of phytoplankton to the interacting effects of iron limitation, light, and temperature by focusing on *T. oceanica*, an open ocean diatom isolate (Figure 5; Sunda and Huntsman, 1995).

In this iteration of CFM-Phyto, increasing temperature increases the maximum growth rate of *T. oceanica*, driving a higher fixed carbon requirement from photosynthetic processes, leading to higher Fe:C ratios (and higher iron requirements) within the cell (Supplementary Figure S2).

Iron limitation is associated with insufficient carriers within the photosynthetic electron transport chain. At high latitudes, phytoplankton acclimate to low light levels by increasing their PSU numbers, leading to higher Fe requirements (Raven, 1990). It follows that phytoplankton in low-light, iron-limited environments (i.e., the Southern Ocean) exhibit iron and light co-limitation (Buitenhuis and Geider, 2010; Schoffman et al., 2016). Under low light, *T. oceanica* is predicted to allocate more of its resources to photosynthetic processes (Figure 5c,d). As observed with temperature, high light conditions support higher growth rates and thus require the synthesis of molecules that support growth.

3.4 Prediction of global *Thalassiosira oceanica* growth rate and elemental stoichiometry

In an effort to predict the biogeography and elemental stoichiometry of the oceanic phytoplankton *T. oceanica*, we evaluate CFM-Phyto output using the climatological average values of dissolved iron, light, and temperature. We also compare the growth and allocation of *T. oceanica* to its neritic relative, *Thalassiosira weissflogii* (Figure 6). In iron-replete open ocean regions, such as the subtropical North Atlantic Gyre, *T. oceanica* experiences a maximum growth rate exceeding 2 d^{-1} (Figure 6a).

It is worth noting that in coastal regions, including the coastal Indian Ocean, along the Benguela and Canary currents in the South Atlantic, and along the Peru current in the South Pacific, lower specific growth rates contrast with relatively high Fe:C ratios. This coincides with more carbon being allocated to photosynthetic processes in these regions (Supplementary Figure S5). This is a result of high K_{dPAR} and lower PAR values in coastal upwelling regions, where high chlorophyll-a concentrations serve as a major attenuator of light (Kirk, 1994). Conversely, low Fe:C ratios are observed in high latitudes. In these regions, cells tend to store carbon due to excess carbon fixation relative to iron uptake. Such carbon storage may be utilized for quick growth when they experience sudden input of iron. Thus, despite there being more iron available in coastal upwelling regions, *T. oceanica* is better able to compete in

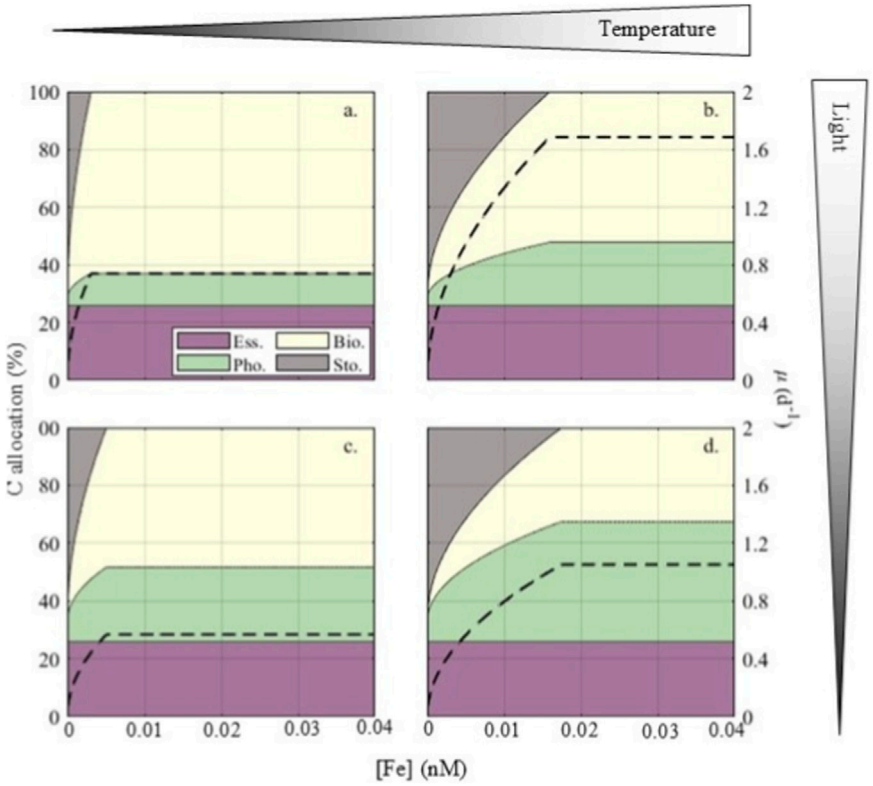

FIGURE 5
Carbon-based macromolecular allocation of *Thalassiosira oceanica* under high light **(a,b)** I = 500 μmol m $^{-2}$s^{-1}), low light **(c,d)** I = 50 μmol m $^{-2}$s^{-1}), high temperature **(b,d)** T = 30 °C), and low temperature **(a,c)** T = 10 °C) conditions. Dotted line represents the specific growth rate.

open ocean regions, where ample light availability encourages high growth rates in species with low iron requirements.

3.5 Comparison to other cellular level models

Our macromolecular model occupies a unique niche in the spectrum of currently available models (Inomura et al., 2020). Developed upon previous versions of the Cell Flux Model (Inomura et al., 2020; Armin and Inomura, 2021), this model resolves macromolecular allocation explicitly and relates it to the cell's overall elemental stoichiometry.

Recent studies show a close relationship between elemental stoichiometry and macromolecular allocation; this model is developed to mechanistically bridge such relationships (Liefer et al., 2019; Liefer et al., 2024). The idea is similar to one of Shuter's classic models (Shuter, 1979), as well as to other more recent models, including those from Geider et al. (1998), Flynn (2001), Pahlow and Oschlies (2009), Bonachela et al. (2013), and Clark et al. (2013); however, there are substantial differences. For example, whereas the model developed by Geider et al. focuses on C:N ratios and functional molecular allocation, our model resolves C:N:P:Fe and the allocation of specific macromolecules, such as proteins and RNA. This aspect of resolving macromolecules in order to group them into functional roles also differentiates our model from those listed above, which solely focus on those larger, functional groups. Furthermore, our model is highly empirical, which also makes it distinctive from some models that are not rigorously tested with experimental data. A comparison of CFM-Phyto to other cellular-level models is provided in the Supplementary Material of Inomura et al. (2020).

3.6 Contribution to earth system models

Current earth system models often represent marine microbes as static stoichiometric reactions. Those that incorporate variable stoichiometry fail to constrain the physiological mechanisms that drive it (Follows et al., 2007; Henson et al., 2022). For example, the Marine Biogeochemistry Library (MARBL), a component of the Community Earth System Model (CESM), relies on coarse-grained relationships between cellular stoichiometry and environmental conditions (Long et al., 2021). In this model, P:C uptake rates of phytoplankton functional types increase linearly with ambient phosphate concentrations until a maximum P:C value is reached. Similarly, Fe:C uptake varies linearly as a function of dissolved iron concentration. This formulation, while more flexible than implicitly modeling microbial growth with fixed stoichiometric ratios, does not provide a mechanistic link to the processes that control their stoichiometric ratios, thus limiting its predictive power. Other recent global models have applied variable stoichiometry without explicitly resolving macromolecules, which are important indicators of cellular functionality (Séférian et al., 2020).

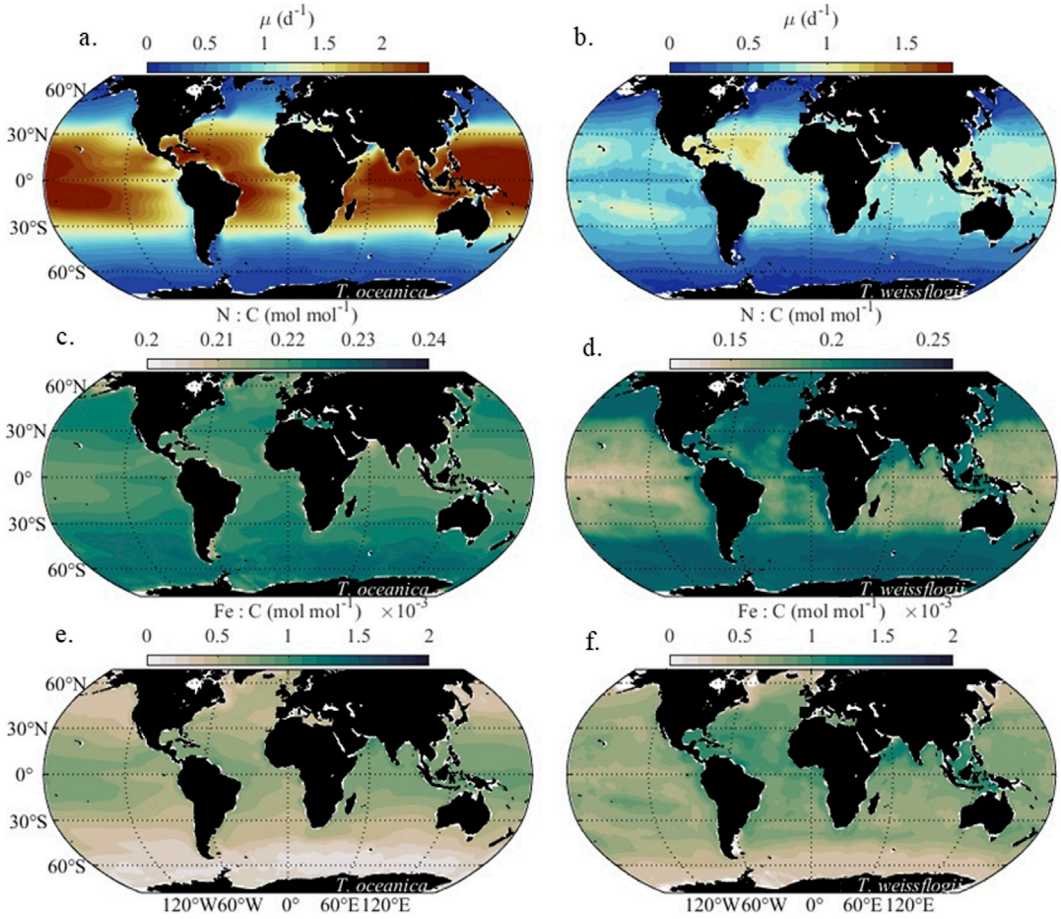

FIGURE 6
Global specific growth rate **(a, b)**, N:C ratios **(c, d)**, and Fe:C ratios **(e, f)** *Thalassiosira oceanica* (left) and *Thalassiosira weissflogii* (right), averaged over the upper 100 m of the water column.

This model provides an additional dimension of phytoplankton physiology, building upon previous efforts. Macromolecular allocation in phytoplankton has been included in a recent simulation on MITgcm (Inomura et al., 2022). The limitation of the MIT-GCM simulation is that it includes only two functional taxa: small and large phytoplankton. This present study brings a more comprehensive empirical relationship to constrain macromolecular allocation under iron limitation across various phytoplankton taxa. In addition, it incorporates the interacting effects of temperature (Equations 9, 10) and light on the allocation and elemental makeup of these taxa. This effort will connect laboratory studies and earth system models more strongly than previous works, facilitating efforts toward simulating the ecophysiology of diverse microorganisms in the global ocean.

4 Conclusion

The Cell Flux Model of Phytoplankton quantifies the impact of dissolved iron concentration on the distribution of macromolecules and elemental ratios within phytoplankton cells. Model output captures the taxon-specific relationship between iron concentration, light levels, temperature, as well as their co-related influences on carbon-based macromolecular allocation. The implementation of iron limitation into a coarse-grained cellular physiology model allows for better characterization of marine microbial distribution and better representation of nutrient cycling for interpretive and predictive models. Future iterations of the model that include luxury iron uptake and storage, as well as nitrogen and iron co-limitation will further improve our understanding of the ecophysiology of various phytoplankton taxa on a global scale.

5 Importance

Despite the importance of iron limitation on phytoplankton growth and physiology within high-latitude marine environments, there exists a gap between observed patterns and their representation in global ecosystem and biogeochemical models. In this paper, we model the effects of dissolved iron on the elemental makeup of various phytoplankton taxa. This research seeks to improve the predictive power of global ocean models through providing a mechanistic understanding of the effects of iron, light,

and temperature co-limitation on phytoplankton physiology and elemental stoichiometry.

Data availability statement

The datasets presented in this study can be found in online repositories. The names of the repository/repositories and accession number(s) can be found in the article/Supplementary Material. The model code used for this study can be found on GitHub at: https://github.com/mkbernish/CFM_Phyto_Iron.

Author contributions

MB: Formal Analysis, Software, Visualization, Writing – original draft, Writing – review and editing. MG: Conceptualization, Data curation, Investigation, Writing – review and editing. JK: Conceptualization, Data curation, Supervision, Writing – review and editing. BP: Data curation, Methodology, Writing – review and editing. KI: Conceptualization, Funding acquisition, Investigation, Methodology, Project administration, Supervision, Writing – review and editing.

Funding

The author(s) declared that financial support was received for this work and/or its publication. This study was supported by the National Science Foundation (OCE-2048373, subaward SUB0000525 from Princeton University, and OCE-2227425 to KI), Rhode Island Science and Technology Advisory Council (AWD14107 to KI) and the Simons Foundation (LS-ECIAMEE-00001549 to KI). We thank these foundations for their support.

Conflict of interest

The author(s) declared that this work was conducted in the absence of any commercial or financial relationships that could be construed as a potential conflict of interest.

Generative AI statement

The author(s) declared that generative AI was not used in the creation of this manuscript.

Any alternative text (alt text) provided alongside figures in this article has been generated by Frontiers with the support of artificial intelligence and reasonable efforts have been made to ensure accuracy, including review by the authors wherever possible. If you identify any issues, please contact us.

Publisher's note

Supplementary material

The Supplementary Material for this article can be found online at: https://www.frontiersin.org/articles/10.3389/feart.2026.1839921/full#supplementary-material

References

Armin, G., and Inomura, K. (2021). Modeled temperature dependencies of macromolecular allocation and elemental stoichiometry in phytoplankton. *Comput. Struct. Biotechnol. J.* 19, 5421–5427. doi:10.1016/j.csbj.2021.09.028

Bonachela, J. A., Allison, S. D., Martiny, A. C., and Levin, S. A. (2013). A model for variable phytoplankton stoichiometry based on cell protein regulation. *Biogeosciences* 10 (6), 4341–4356. doi:10.5194/bg-10-4341-2013

Boyd, P. W., Jickells, T., Law, C. S., Blain, S., Boyle, E. A., Buesseler, K. O., et al. (2007). Mesoscale iron enrichment experiments 1993-2005: synthesis and future directions. *Science* 315 (5812), 612–617. doi:10.1126/science.1131669

Breitbarth, E., Achterberg, E. P., Ardelan, M., Baker, A. R., Bucciarelli, E., Chever, F., et al. (2010). Iron biogeochemistry across marine systems–progress from the past decade. *Biogeosciences* 7 (3), 1075–1097. doi:10.5194/bg-7-1075-2010

Bremer, H. D. P. P., and Dennis, P. P. (1996). Modulation of chemical composition and other parameters of the cell by growth rate. *Escherichia coli Salmonella Cellular Molecular Biology* 2 (2), 1553–1569.

Buitenhuis, E. T., and Geider, R. J. (2010). A model of phytoplankton acclimation to iron–light colimitation. *Limnol. Oceanogr.* 55 (2), 714–724. doi:10.4319/lo.2009.55.2.0714

Chalup, M. S., and Laws, E. A. (1990). A test of the assumptions and predictions of recent microalgal growth models with the marine phytoplankter Pavlova lutheri. *Limnol. Oceanogr.* 35 (3), 583–596. doi:10.4319/lo.1990.35.3.0583

Clark, J. R., Lenton, T. M., Williams, H. T., and Daines, S. J. (2013). Environmental selection and resource allocation determine spatial patterns in picophytoplankton cell size. *Limnol. Oceanogr.* 58 (3), 1008–1022. doi:10.4319/lo.2013.58.3.1008

Cullen, J. J. (1990). On models of growth and photosynthesis in phytoplankton. *Deep Sea Res. Part A. Oceanogr. Res. Pap.* 37 (4), 667–683. doi:10.1016/0198-0149(90)90097-f

Eppley, R. W., and Peterson, B. J. (1979). Particulate organic matter flux and planktonic new production in the deep ocean. *Nature* 282 (5740), 677–680. doi:10.1038/282677a0

Faizi, M., Zavřel, T., Loureiro, C., Červený, J., and Steuer, R. (2018). A model of optimal protein allocation during phototrophic growth. *Biosystems* 166, 26–36. doi:10.1016/j.biosystems.2018.02.004

Feng, Y., Hare, C. E., Rose, J. M., Handy, S. M., DiTullio, G. R., Lee, P. A., et al. (2010). Interactive effects of iron, irradiance and CO_2 on ross sea phytoplankton. *Deep Sea Res. Part I Oceanogr. Res. Pap.* 57 (3), 368–383. doi:10.1016/j.dsr.2009.10.013

Field, C. B., Behrenfeld, M. J., Randerson, J. T., and Falkowski, P. (1998). Primary production of the biosphere: integrating terrestrial and oceanic components. *Science* 281 (5374), 237–240. doi:10.1126/science.281.5374.237

Finkel, Z. V., Follows, M. J., Liefer, J. D., Brown, C. M., Benner, I., and Irwin, A. J. (2016). Phylogenetic diversity in the macromolecular composition of microalgae. *PLoS One* 11 (5), e0155977. doi:10.1371/journal.pone.0155977

Flynn, K. J. (2001). A mechanistic model for describing dynamic multi-nutrient, light, temperature interactions in phytoplankton. *J. Plankton Res.* 23 (9), 977–997. doi:10.1093/plankt/23.9.977

Follows, M. J., Dutkiewicz, S., Grant, S., and Chisholm, S. W. (2007). Emergent biogeography of microbial communities in a model ocean. *Science* 315 (5820), 1843–1846. doi:10.1126/science.1138544

Geider, R. J., and La Roche, J. (2002). Redfield revisited: variability of C:N:P in marine microalgae and its biochemical basis. *Eur. J. Phycol.* 37 (1), 1–17. doi:10.1017/s0967026201003456

Geider, R. J., MacIntyre, H. L., and Kana, T. M. (1998). A dynamic regulatory model of phytoplanktonic acclimation to light, nutrients, and temperature. *Limnol. Oceanography* 43 (4), 679–694. doi:10.4319/lo.1998.43.4.0679

Hastings, W. K. (1970). *Monte Carlo Sampling Methods Using Markov Chains and Their Applications*.

Healey, F. P. (1985). Interacting effects of light and nutrient limitation on the growth rate of *Synechococcus linearis* (Cyanophyceae) 1. *J. Phycology* 21 (1), 134–146. doi:10.1111/j.0022-3646.1985.00134.x

Henson, S. A., Laufkötter, C., Leung, S., Giering, S. L., Palevsky, H. I., and Cavan, E. L. (2022). Uncertain response of ocean biological carbon export in a changing world. *Nat. Geosci.* 15 (4), 248–254. doi:10.1038/s41561-022-00927-0

Huang, Y., Tagliabue, A., and Cassar, N. (2022). Data-driven modeling of dissolved iron in the global ocean. *Front. Mar. Sci.* 9, 837183. doi:10.3389/fmars.2022.837183

Inomura, K., Omta, A. W., Talmy, D., Bragg, J., Deutsch, C., and Follows, M. J. (2020). A mechanistic model of macromolecular allocation, elemental stoichiometry, and growth rate in phytoplankton. *Front. Microbiol.* 11, 86. doi:10.3389/fmicb.2020.00086

Inomura, K., Deutsch, C., Jahn, O., Dutkiewicz, S., and Follows, M. J. (2022). Global patterns in marine organic matter stoichiometry driven by phytoplankton ecophysiology. *Nat. Geosci.* 15 (12), 1034–1040. doi:10.1038/s41561-022-01066-2

Jabre, L., and Bertrand, E. M. (2020). Interactive effects of iron and temperature on the growth of *fragilariopsis Cylindrus*. *Limnol. Oceanogr. Lett.* 5 (5), 363–370. doi:10.1002/lol2.10158

Jahn, M., Vialas, V., Karlsen, J., Maddalo, G., Edfors, F., Forsström, B., et al. (2018). Growth of Cyanobacteria is constrained by the abundance of light and carbon assimilation proteins. *Cell Rep.* 25 (2), 478–486. doi:10.1016/j.celrep.2018.09.040

Kim, J., Armin, G., and Inomura, K. (2022). Saturating relationship between phytoplankton growth rate and nutrient concentration explained by macromolecular allocation. *Curr. Res. Microb. Sci.* 3, 100167. doi:10.1016/j.crmicr.2022.100167

Kirk, J. T. (1994). *Light and Photosynthesis in Aquatic Ecosystems*. Cambridge University Press.Cambridge.

Liefer, J. D., Garg, A., Fyfe, M. H., Irwin, A. J., Benner, I., Brown, C. M., et al. (2019). The macromolecular basis of phytoplankton C: N: p under nitrogen starvation. *Front. Microbiol.* 10, 763. doi:10.3389/fmicb.2019.00763

Liefer, J. D., White, A. E., Finkel, Z. V., Irwin, A. J., Dugenne, M., Inomura, K., et al. (2024). Latitudinal patterns in ocean C: N: p reflect phytoplankton acclimation and macromolecular composition. *Proc. Natl. Acad. Sci.* 121 (46), e2404460121. doi:10.1073/pnas.2404460121

Long, M. C., Moore, J. K., Lindsay, K., Levy, M., Doney, S. C., Luo, J. Y., et al. (2021). Simulations with the marine biogeochemistry library (MARBL). *J. Adv. Model. Earth Syst.* 13 (12), e2021MS002647. doi:10.1029/2021ms002647

Metropolis, N., Rosenbluth, A. W., Rosenbluth, M. N., Teller, A. H., and Teller, E. (1953). Equation of state calculations by fast computing machines. *J. Chem. Phys.* 21 (6), 1087–1092. doi:10.1063/1.1699114

Morel, A. (1988). Optical modeling of the upper ocean in relation to its biogenous matter content (case I waters). *J. Geophysical Research Oceans* 93 (C9), 10749–10768. doi:10.1029/jc093ic09p10749

Nicklisch, A., and Steinberg, C. E. (2009). RNA/protein and RNA/DNA ratios determined by flow cytometry and their relationship to growth limitation of selected planktonic algae in culture. *Eur. J. Phycol.* 44 (3), 297–308. doi:10.1080/09670260802578518

Pahlow, M., and Oschlies, A. (2009). Chain model of phytoplankton P, N and light colimitation. *Mar. Ecol. Prog. Ser.* 376, 69–83. doi:10.3354/meps07748

Raven, J. A. (1990). Predictions of Mn and Fe use efficiencies of phototrophic growth as a function of light availability for growth and of C assimilation pathway. *New Phytol.* 116 (1), 1–18. doi:10.1111/j.1469-8137.1990.tb00505.x

Reagan, J. R., Boyer, T. P., García, H. E., Locarnini, R. A., Baranova, O. K., Bouchard, C., et al. (2024). *World Ocean Atlas 2023*. NOAA National Centers for Environmental Information.

Regaudie-de-Gioux, A., and Duarte, C. M. (2012). Temperature dependence of planktonic metabolism in the ocean. *Glob. Biogeochem. Cycles* 26 (1). doi:10.1029/2010gb003907

Rhee, G. Y. (1978). Effects of N: p atomic ratios and nitrate limitation on algal growth, cell composition, and nitrate uptake 1. *Limnol. Oceanography* 23 (1), 10–25. doi:10.4319/lo.1978.23.1.0010

Saito, M. A., Bertrand, E. M., Dutkiewicz, S., Bulygin, V. V., Moran, D. M., Monteiro, F. M., et al. (2011). Iron conservation by reduction of metalloenzyme inventories in the marine diazotroph Crocosphaera watsonii. *Proc. Natl. Acad. Sci.* 108 (6), 2184–2189. doi:10.1073/pnas.1006943108

Schoffman, H., Lis, H., Shaked, Y., and Keren, N. (2016). Iron–nutrient interactions within phytoplankton. *Front. Plant Sci.* 7, 1223. doi:10.3389/fpls.2016.01223

Scott, M., Gunderson, C. W., Mateescu, E. M., Zhang, Z., and Hwa, T. (2010). Interdependence of cell growth and gene expression: origins and consequences. *Science* 330 (6007), 1099–1102. doi:10.1126/science.1192588

Séférian, R., Berthet, S., Yool, A., Palmiéri, J., Bopp, L., Tagliabue, A., et al. (2020). Tracking improvement in simulated marine biogeochemistry between CMIP5 and CMIP6. *Curr. Clim. Change Rep.* 6 (3), 95–119. doi:10.1007/s40641-020-00160-0

Shuter, B. (1979). A model of physiological adaptation in unicellular algae. *J. Theor. Biol.* 78 (4), 519–552. doi:10.1016/0022-5193(79)90189-9

Son, S., and Wang, M. (2015). Diffuse attenuation coefficient of the photosynthetically available radiation Kd (PAR) for global open ocean and coastal waters. *Remote Sens. Environ.* 159, 250–258. doi:10.1016/j.rse.2014.12.011

Steinacher, M., Joos, F., Frölicher, T., Bopp, L., Cadule, P., Cocco, V., et al. (2010). Projected 21st century decrease in marine productivity: a multi-model analysis. *Biogeosciences* 7 (3), 979–1005. doi:10.5194/bg-7-979-2010

Strzepek, R. F., Boyd, P. W., and Sunda, W. G. (2019). Photosynthetic adaptation to low iron, light, and temperature in Southern Ocean phytoplankton. *Proc. Natl. Acad. Sci.* 116 (10), 4388–4393. doi:10.1073/pnas.1810886116

Sunda, W. G., and Huntsman, S. A. (1995). Iron uptake and growth limitation in oceanic and coastal phytoplankton. *Mar. Chem.* 50 (1–4), 189–206. doi:10.1016/0304-4203(95)00035-p

Sunda, W. G., and Huntsman, S. A. (1997). Interrelated influence of iron, light and cell size on marine phytoplankton growth. *Nature* 390 (6658), 389–392. doi:10.1038/37093

Sunda, W. G., and Huntsman, S. A. (2011). Interactive effects of light and temperature on iron limitation in a marine diatom: implications for marine productivity and carbon cycling. *Limnol. Oceanogr.* 56 (4), 1475–1488. doi:10.4319/lo.2011.56.4.1475

Tagliabue, A., Williams, R. G., Rogan, N., Achterberg, E. P., and Boyd, P. W. (2014). A ventilation-based framework to explain the regeneration-scavenging balance of iron in the ocean. *Geophys. Res. Lett.* 41 (20), 7227–7236. doi:10.1002/2014gl061066

Tanioka, T., and Matsumoto, K. (2020). A meta-analysis on environmental drivers of marine phytoplankton C: N: p. *Biogeosciences* 17 (11), 2939–2954. doi:10.5194/bg-17-2939-2020

Taylor, A. H., Geider, R. J., and Gilbert, F. J. (1997). Seasonal and latitudinal dependencies of phytoplankton carbon-to-chlorophyll a ratios: results of a modelling study. *Mar. Ecol. Prog. Ser.* 152, 51–66. doi:10.3354/meps152051

Zavřel, T., Faizi, M., Loureiro, C., Poschmann, G., Stühler, K., Sinetova, M., et al. (2019). Quantitative insights into the cyanobacterial cell economy. *Elife* 8, e42508. doi:10.7554/eLife.42508